The Astrophysical Journal, 741:43 (7pp), 2011 November 1 doi:10.1088/0004-637X/741/1/43

THE ROLE OF ALPHA PARTICLES IN THE EVOLUTION OF THE SOLAR-WIND TURBULENCE TOWARD SHORT SPATIAL SCALES

D. Perrone, F. Valentini, and P. Veltri
Dipartimento di Fisica and CNISM, Università della Calabria, I-87030 Rende (CS), Italy
Received 2011 May 30; accepted 2011 August 2; published 2011 October 13

ABSTRACT

We present a numerical study of the kinetic dynamics of protons and alpha particles during the evolution of the solar-wind turbulent cascade, in which the energy injected in large-scale slab-type Alfvénic fluctuations is transferred toward short spatial scale lengths, across the proton skin depth. We make use of a hybrid Vlasov–Maxwell code that integrates numerically the Vlasov equation for both the ion species, while the electrons are considered as a fluid. The system evolution is investigated in terms of different values of the electron to proton and alpha particle to proton temperature ratios. The numerical results show that the previously studied kinetic dynamics of protons is not strongly affected by the presence of alpha particles, at least when they are present in low concentration. Our simulations not only provide a physical explanation for the generation of beams of accelerated particles along the direction of the ambient magnetic field for both protons and alpha particles, but also show that this mechanism is more efficient for protons than for alpha particles, in agreement with recent solar-wind data analyses.

Key words: acceleration of particles – methods: numerical – solar wind – turbulence – waves

Online-only material: color figures

1. INTRODUCTION

Helium is the second most abundant element in the Sun and, for this reason, plays an important and not fully understood role in the dynamics of the solar wind, corona, and interior. In situ solar-wind measurements have clearly shown that the heavy minor ions are heated and accelerated preferentially as compared to protons and electrons. These observations indicate that there exist sources of ion heating and momentum exchange which operate differently on protons and alpha particles throughout the solar wind (Hansteen et al. 1997; Kasper et al. 2008).

The physical mechanisms responsible for this phenomenology are not yet identified, and their interpretation could provide key insights into understanding why the temperature of the outer solar atmosphere and expanding corona forming the solar wind is two or three orders of magnitude higher than that of the photosphere. Ion cyclotron (IC) waves, originated from the Sun, are usually considered the source of heating and acceleration of minor ions. Indeed, the IC resonant interaction has different resonance factors for the protons and alpha particles and thereby yields different momentum and energy transfer rates for the two species (Hollweg & Isenberg 2002).

The investigation of this preferential source has been the subject of several analytical studies focused on the quasi-linear resonant cyclotron interaction of solar-wind ions with parallel-propagating IC waves (Dusenbery & Hollweg 1981; Marsch et al. 1982; Isenberg & Hollweg 1983), but none of these works includes the effects of solar-wind alpha particles in the wave dispersion relations. The presence of heavy ions can drastically affect the IC dispersion relation in the vicinity of the IC frequency. In the limit of parallel propagation, the waves at frequencies close to the cyclotron frequency can interact with the heavy ions comoving with the bulk plasma (Isenberg 1984).

In the solar wind, the energy of magnetic and electric fluctuations is transferred from large wavelengths to short wavelengths along a turbulent cascade, and then in principle reaches high frequencies. When the energy is carried at frequencies of the order of the cyclotron frequency the resonant IC interaction can occur. Nevertheless, whether the turbulence in realistic solar-wind conditions can deliver enough energy to frequencies of the order of the IC frequency in such a way as to produce the cyclotron heating still represents an unanswered question.

In 2004, Dmitruk et al. (2004) performed numerical experiments of test particle energization inside a turbulent magneto-hydrodynamic cascade. The magnetic and electric fields are obtained from pseudo-spectral direct numerical solutions of compressible three-dimensional magnetohydrodynamic equations in the presence of a strong background magnetic field. Interaction of particles with small-scale fluctuations gives rise to efficient acceleration but not by cyclotron resonance. In the same scenario, Parashar et al. (2009) studied the kinetic evolution of the Orszag–Tang vortex by means of two-dimensional collisionless particle-in-cell (PIC) simulations in the hybrid regime, with mean magnetic field out of the simulation plane. While at large scales the evolution of the energy spectra is similar to that recovered in the magnetohydrodynamics regime, at short wavelengths the system evolution leads to the heating of protons in the direction perpendicular to the background magnetic field, thus producing a temperature anisotropy of the type observed in the corona and the solar wind. The perpendicular heating occurs without any obvious connection to classical cyclotron resonances, which require wavevectors parallel to the background magnetic field.

Xie et al. (2004) studied the interaction of protons and multiple minor ions (He^{++}, O^{5+}) with Alfvén cyclotron fluctuation spectra in the corona and the solar wind. These authors performed one-dimensional hybrid PIC simulations to study the evolution of an initially homogeneous, collisionless, magnetized plasma in the presence of an assigned spectrum of waves propagating parallel to the background magnetic field. The energy of the initial perturbations is injected directly at frequencies close to the cyclotron frequency of the minor ions, thus efficiently triggering the resonant interaction and producing the particle heating.

More recently, Ofman (2010) has studied the heating and the acceleration of a multi-ion plasma in the solar wind by a turbulent spectrum of Alfvénic fluctuations, using a two-dimensional hybrid PIC numerical model that includes an

input turbulent wave spectrum guided by observations with inhomogeneous background density. The frequency band of the waves was below the proton gyro-resonant frequency but once again included the alpha gyro-resonant frequency in the plasma rest frame.

Nowadays, the increasing computational power of modern supercomputers allows one to run kinetic Eulerian Vlasov codes (Mangeney et al. 2002; Valentini et al. 2007) that solve the Vlasov–Maxwell equations in multidimensional phase space. These simulations represent an important tool for the interpretation of many physical phenomena recovered in spacecraft observations, such as, for example, the complex phenomenology observed in the high-frequency region of the energy spectra. Indeed, the Eulerian low-noise algorithms give the possibility, for the first time, of analyzing the kinetic effects in the tail at short spatial scales of the energy spectra, where the energy level of the small-scale fluctuations is typically very low. In this spectral region, the statistical noise introduced by the Lagrangian PIC algorithms would crucially affect the numerical results.

In recent years, hybrid Vlasov–Maxwell simulations in 1D-3V (one dimension in physical space and three dimensions in velocity space; Valentini et al. 2008, 2011; Valentini & Veltri 2009; Marradi et al. 2010) and 2D-3V (Valentini et al. 2010) phase space configuration, in which the Vlasov equation is solved for the proton species while electrons are considered as a fluid, allowed significant steps forward to be made in the analysis of the evolution of solar-wind "slab" turbulence toward small wavelengths. In fact, these numerical results have shown that a newly identified electrostatic (acoustic-like) branch of waves, called ion-bulk (IBk) waves, longitudinal with respect to the average magnetic field and driven by particle distribution functions far from the local thermodynamic equilibrium, represents a privileged channel to carry the energy toward small scales. Moreover, the resonant interaction of protons with IC waves triggers a physical mechanism that leads to the generation of a field-aligned proton beam, whose mean velocity is close to V_A, independently of the electron to proton temperature ratio T_e/T_p. The generation of this secondary proton beam is a typical feature detected in many solar-wind spacecraft observations (see, for example, Marsch et al. 1982).

In this paper, a new version of the hybrid Vlasov–Maxwell code, where the Vlasov equation is integrated both for the proton and the alpha particle distribution functions, is used to study the role of minor ions in the evolution of the solar-wind turbulent cascade self-consistently generated at large wavelengths by nonlinear wave–wave interactions. The system dynamics is investigated using a parameter set which fits the plasma solar-wind conditions and by varying the electron to proton T_e/T_p and alpha particle to proton T_α/T_p temperature ratios. Our numerical results reproduce many aspects of the complex phenomenology recovered in many spacecraft observations (Marsch 2010; Bourouaine et al. 2011) in the solar wind, such as the generation of field-aligned beams of accelerated particles (both protons and alpha particles) in the direction of the ambient magnetic field.

2. NUMERICAL MODEL

We use the hybrid Vlasov–Maxwell code in 1D-3V phase space configuration to model a collisionless and magnetized plasma. The ions (protons and alpha particles) are treated as kinetic particles, so the Vlasov equation is integrated for the proton and alpha particle distribution functions, while the electron response is taken into account through a generalized Ohm's law for the electric field, which retains Hall and electron inertia effects. We consider a low-frequency approximation that consists in neglecting the displacement current in Ampère's law. The Faraday equation and an isothermal equation of state for the electron pressure close the system. The quasi-neutrality condition is imposed by setting $n_e \simeq n_p + Z_\alpha n_\alpha$, where n_e, n_p, and n_α are the particle density of electrons, protons, and alpha particles, respectively, and Z_α is the charge number for the alpha particles.

From now on, times are scaled by the proton-cyclotron frequency $\Omega_{\rm cp}$, velocities by the Alfvén speed $V_A = B_0/\sqrt{4\pi\rho}$ (B_0 being the background magnetic field and ρ the initial homogeneous proton mass density), lengths by the proton skin depth $d_p = V_A/\Omega_{\rm cp}$, and masses by the proton mass m_p. The explicit expression for Ohm's equation in dimensionless units is written as follows:

$$\mathbf{E} - d_e^2 \Delta \mathbf{E} = -(\mathbf{u}_e \times \mathbf{B}) - \frac{1}{n_e}\nabla P_e - \sum_i \frac{N_i}{M_i}(\mathbf{u}_i \times \mathbf{B}) + \frac{1}{n_e}\sum_i \frac{1}{M_i}\nabla \cdot \mathbf{\Pi}_i + d_e^2 \nabla \cdot \Big[\sum_i N_i \mathbf{u}_i \mathbf{u}_i - \mathbf{u}_e \mathbf{u}_e\Big], \quad (1)$$

where the subscript $i = p, \alpha$ stands for protons and alpha particles, respectively, $N_i = Z_i n_i/n_e$, and $1/M_i = Z_i m_e/m_i$, with m_e and m_i being the electron and ion masses. In Equation (1) the ion density n_i, the ion bulk velocity $\mathbf{u}_i$, and the ion pressure tensor $\mathbf{\Pi}_i$ are calculated as the velocity moments of the distribution function, while the electron bulk velocity is given by $\mathbf{u}_e = (\sum_i Z_i n_i \mathbf{u}_i - \nabla \times \mathbf{B})/n_e$. The electron skin depth d_e in scaled units is equal to $\sqrt{m_e/m_p}$.

We simulate a plasma embedded in a background magnetic field $\mathbf{B}_0 = B_0 \mathbf{e}_x$, where x is the direction of wave propagation. Protons and alpha particles have Maxwellian velocity distributions and homogenous density at $t = 0$. To mimic the slab turbulence the initial equilibrium configuration is perturbed by a set of Alfvénic fluctuations circularly polarized in the plane perpendicular to $\mathbf{B}_0$ and propagating along it. The form of velocity and magnetic perturbations ($\delta u_{y,p}$, $\delta u_{z,p}$, $\delta u_{y,\alpha}$, $\delta u_{z,\alpha}$, δB_y, and δB_z) was derived from the linearized three-fluid equations (electrons, protons, and alpha particles):

$$\begin{cases} \delta u_{y,p} = -\sum_n \epsilon_n \frac{1}{\omega_n - 1} \cos(k_n x) \\ \delta u_{z,p} = -\sum_n \epsilon_n \frac{1}{\omega_n - 1} \sin(k_n x) \end{cases} \quad (2)$$

$$\begin{cases} \delta u_{y,\alpha} = -\sum_n \frac{Z_\alpha m_p}{m_\alpha} \epsilon_n \frac{1}{\omega_n - Z_\alpha m_p/m_\alpha} \cos(k_n x) \\ \delta u_{z,\alpha} = -\sum_n \frac{Z_\alpha m_p}{m_\alpha} \epsilon_n \frac{1}{\omega_n - Z_\alpha m_p/m_\alpha} \sin(k_n x) \end{cases} \quad (3)$$

$$\begin{cases} \delta B_y = -\sum_n \epsilon_n \frac{k}{\omega_n} \cos(k_n x) \\ \delta B_z = -\sum_n \epsilon_n \frac{k}{\omega_n} \sin(k_n x), \end{cases} \quad (4)$$

where ϵ_n is the amplitude of the nth mode and ω_n is its frequency. The solution for the wave frequency as a function of the wavenumber is displayed in Figure 1, where we show the k–ω diagrams for right-handed (a) and left-handed (b) polarized waves in parallel propagation, obtained for a percentage of alpha particles with respect to protons equal to 5%. We note that for the case of left-handed polarized waves the presence of alpha particles, even in a small amount, produces a split of the solutions (see black (1) and red (2) lines in panel (b)) with respect to the case of a pure electron–proton plasma.

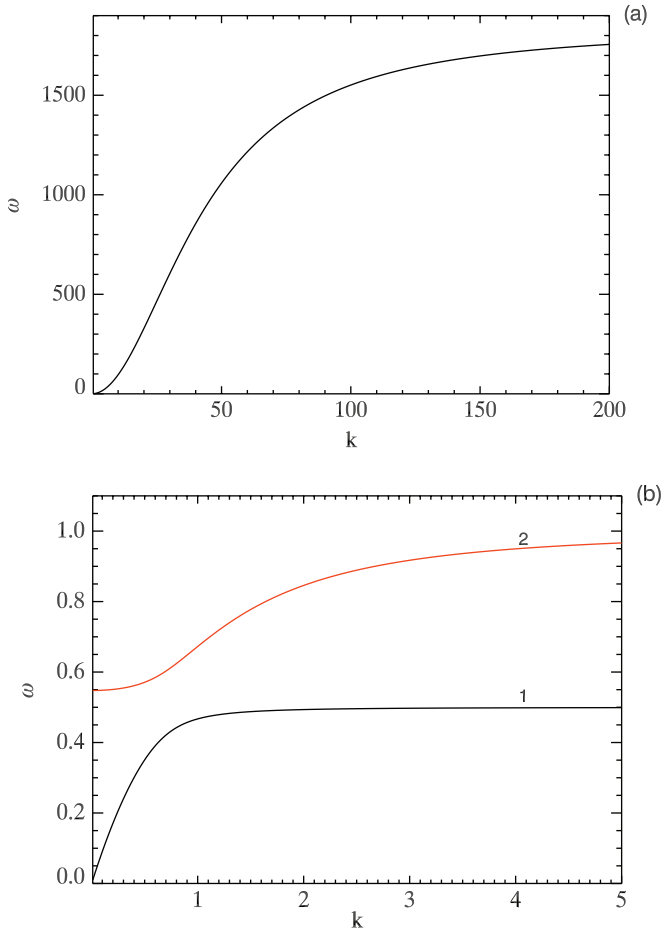

Figure 1. k–ω diagrams for right-handed (a) and left-handed (b) polarized waves in parallel propagation.

(A color version of this figure is available in the online journal.)

The isothermal equation of state for the electron pressure in scaled units is $P_e = (\beta/2) n_e T_e/T_p$, where $\beta_p = 2v_{\mathrm{th},p}^2/v_A^2$ ($v_{\mathrm{th},p} = \sqrt{T_p/m_p}$ being the proton thermal speed) is the plasma beta. The value of the plasma beta is fixed at $\beta_p = 0.5$ and consequently the proton thermal speed is a half of the Alfvén speed $v_{\mathrm{th},p} = 0.5$. The electron to proton mass ratio is $m_e/m_p = 1/1836$, the alpha particle to proton mass ratio is $m_\alpha/m_p = 4$, and $Z_\alpha = 2$; the density ratio between alpha particles and protons is fixed at $n_{0,\alpha}/n_{0,p} = 5\%$. The length of the numerical spatial domain is $L_x = 12.8 \times 2\pi d_p = 80.4 d_p$, while the limits of the velocity domain in each direction are fixed at $v_{i,\max} = 5 v_{\mathrm{th},i}$. We use 4096 grid points in physical space, where periodic boundary conditions are imposed, and 51^3 in velocity space.

Only the first three modes in the spectrum of velocity and magnetic perturbations are excited at $t = 0$, in such a way that the resulting perturbation amplitude is $A = 0.5$. The energy is injected at $t = 0$ at wavenumbers in the range $0.078 \lesssim k \lesssim 0.23$, along the left-hand branch 1 in Figure 1(b) and no density disturbances are initially imposed on the system. The time step Δt has been chosen in such a way that the Courant–Friedrichs–Lewy condition for the numerical stability of the Vlasov algorithm is satisfied (Peyret & Taylor 1986).

3. NUMERICAL RESULTS

We numerically analyze the kinetic dynamics of protons and alpha particles when the energy is transferred from large to short wavelengths along the solar-wind turbulent cascade, in terms of different values of the temperature ratios T_e/T_p and T_α/T_p. For the choice of the values of T_α/T_p, we refer to the work by Kasper et al. (2008), who discussed the breakdown of temperature equilibrium between hydrogen and helium in the solar-wind data from Faraday Cup instruments on the *Wind* spacecraft. They showed that the distribution of the temperature ratio displays two maxima: the first at $T_\alpha/T_p = 1$, consistent with an isothermal fluid wind, and the second at $T_\alpha/T_p = 4$, where the two species instead have equal thermal speeds. For this reason, we performed simulations using these values of the alpha particle to proton temperature ratio. For the electron to proton temperature ratio, we use the values $T_e/T_p = 1, 5,$ and 10. Typical values of T_e/T_p for the solar-wind plasma are in the range $0.5 < T_e/T_p < 4$ (Schwenn & Marsch 1991).

Independently of T_e/T_p or T_α/T_p, in the early stage of the system evolution ($0 < t < 30$), both the proton and the alpha particle distribution functions display the generation of perpendicular temperature anisotropy, due to resonant interaction of ions with left-hand polarized IC waves (Arunasalam 1976; Busnardo-Neto et al. 1976). The maximum value of the anisotropy index, defined as $\eta = \langle T_\perp \rangle_x / \langle T_\parallel \rangle_x$ ($\langle \ldots \rangle_x$ indicates a spatial average), is $\eta = 1.2$ for alpha particles and $\eta = 1.06$ for protons. The reason for this larger temperature anisotropy for alpha particles with respect to protons is due to the fact that in our simulations the energy is injected into the system at $t = 0$ along the left-hand branch 1 in Figure 1(b) that saturates at frequencies of the order of the cyclotron frequency of the alpha particles ($\Omega_{c\alpha} = \Omega_{cp}/2 = 0.5$).

By comparing the time evolution of the electric and magnetic energies for all the values of the electron to proton and alpha particle to proton temperature ratios, we realized that in the high wavenumbers range of the spectrum, say $k > 10$, the level of the electric fluctuations is about five orders of magnitude higher than that of the magnetic ones; moreover, we noticed that short-scale structures are generated in the longitudinal component of the electric field. On the basis of the considerations above, we conclude that the tail at short wavelengths of the energy spectrum is dominated by electrostatic activity.

In Figure 2(a), we report the time evolution of the longitudinal electric energy at short wavelengths, defined as $\mathcal{E}(t) = \sum_k |E_{k_x}|^2$ (with $k > 10$), in a semilogarithmic plot for the case $T_e/T_p = 1$ and with $T_\alpha/T_p = 1$ (black line (1)) and $T_\alpha/T_p = 4$ (red line (2)). From the time history of $\mathcal{E}$, one sees that a sudden exponential increase occurs for both cases $T_\alpha/T_p = 1, 4$. We point out that for $T_\alpha/T_p = 4$ this exponential growth is somewhat delayed with respect to the case $T_\alpha/T_p = 1$. After the growing phase, both signals reach a saturation level (higher for $T_\alpha/T_p = 1$), remain almost constant for a short time, and then start decreasing up to a complete dissipation. As recently discussed in Valentini et al. (2011), the exponential growth observed in Figure 2(a) is trigged by the generation, through the IC resonant interaction, of regions of positive slope (bumps) in the longitudinal velocity distribution of protons, while the dissipation phase is presumably due to the fact that the energy injected into the system at $t = 0$ is not replenished during our simulations of decay turbulence. Figure 2(b) shows the k–ω spectrum of the parallel electric energy for the case $T_\alpha/T_p = 1$, evaluated in the time interval $310 < t < 370$, where the saturation level is recovered (see black line (1) in Figure 2(a)). This Fourier spectrum shows that the short-scale electrostatic activity consists of an acoustic branch of waves (IBk waves) with phase speed $v_\phi^{(\mathrm{IBk})}$ comparable to the proton thermal velocity ($v_\phi^{(\mathrm{IBk})} \simeq 1.24 v_{\mathrm{th},p}$).

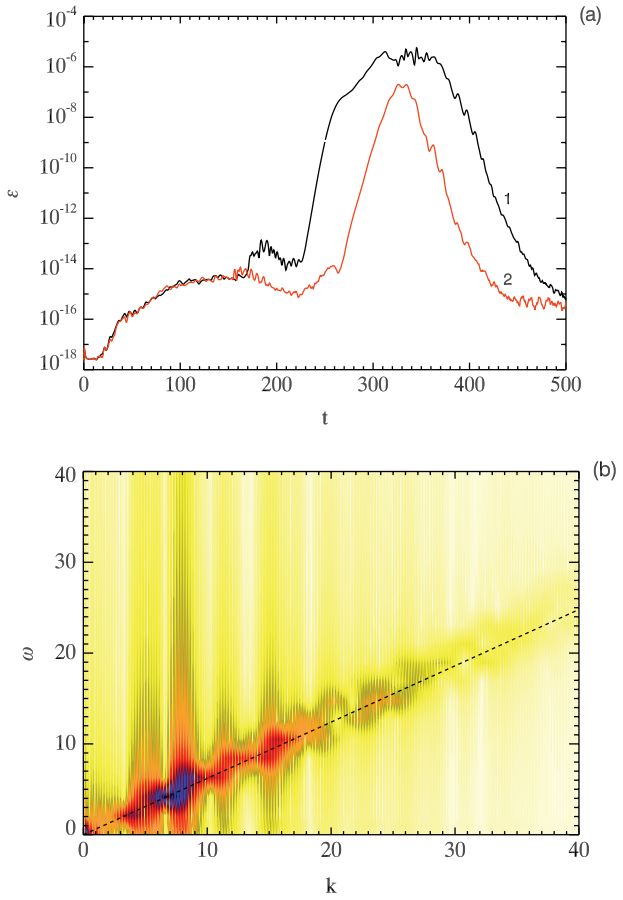

Figure 2. (a) Time evolution of $\mathcal{E}$ in a semilogarithmic plot for the case $T_e/T_p = 1$ and with $T_\alpha/T_p = 1$ (black line (1)) and $T_\alpha/T_p = 4$ (red line (2)). (b) Numerical k–ω spectrum of parallel electric energy at $t = 336$, for the case $T_e/T_p = 1$ and with $T_\alpha/T_p = 1$. The black dashed line represents the phase speed of the IBk waves ($v_\phi^{(\mathrm{IBk})} \sim 1.24 v_{\mathrm{th},p}$).

(A color version of this figure is available in the online journal.)

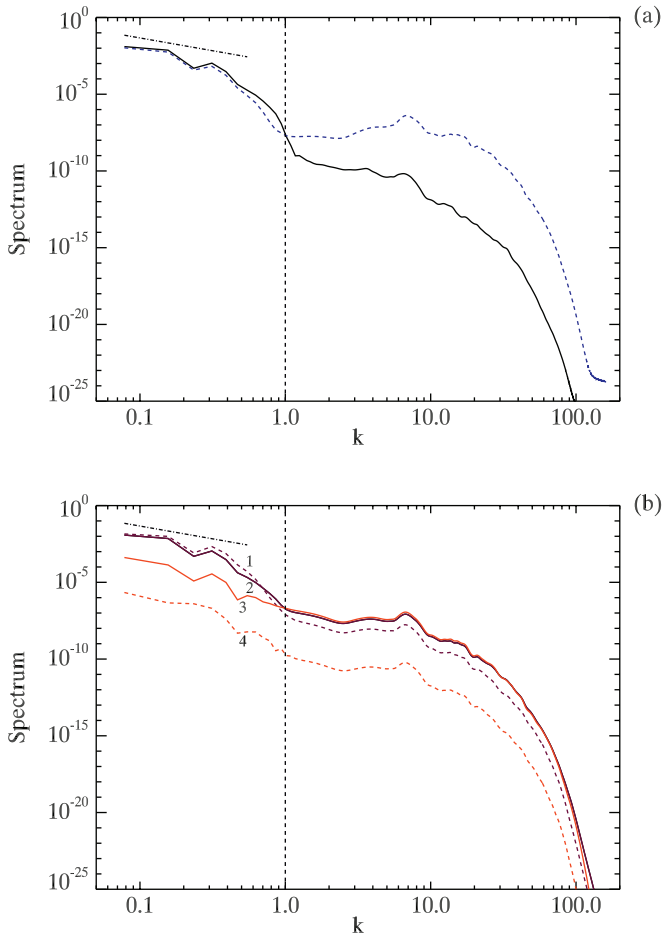

Figure 3. (a) Energy spectra for electric (blue dashed line) and magnetic (black solid line) fluctuations, for a simulation with $T_e/T_p = 1$ and with $T_\alpha/T_p = 1$, time averaged in the interval $310 < t < 370$. (b) The corresponding spectra for proton kinetic energy (purple solid line (2)), proton density (red solid line (3)), alpha particle kinetic energy (purple dashed line (1)), and alpha particle density (red dashed line (4)). In both panels the dot-dashed line at $0.1 \lesssim k \lesssim 0.5$ indicates the Kolmogorov $k^{-5/3}$ expectation, while the vertical dashed line indicates the proton skin depth wavenumber.

(A color version of this figure is available in the online journal.)

The same evidence has been found for the case $T_\alpha/T_p = 4$ (not shown here).

In Figure 3, we show the energy spectra for the case $T_e/T_p = 1$ and $T_\alpha/T_p = 1$. In panel (a), we report the spectra of electric (blue dashed line) and magnetic (black solid line) fluctuations averaged in the time interval $310 < t < 370$, where the maximum activity is observed in Figure 2(a) (black line (1)). We point out that in the range of large wavenumbers the electric energy is about four orders of magnitude higher than the magnetic one, indicating that electrostatic activity is recovered at short scales. In panel (b), we report the corresponding spectra for proton kinetic energy (purple solid line (2)), proton density (red solid line (3)), alpha particle kinetic energy (purple dashed line (1)), and alpha particle density (red dashed line (4)). The fact that the spectra for proton density and proton kinetic energy fluctuations are evidently coupled in the short-scale range of the energy spectra is a signature of the presence of acoustic-like fluctuations. In both panels the dot-dashed lines in the small wavenumber range of the spectra indicate the Kolmogorov $k^{-5/3}$ expectation, reported only for reference purposes.

In order to investigate the effect of the propagation of these electrostatic acoustic-type fluctuations on the particle distribution functions, in Figure 4(a) we report the longitudinal (x–v_x) phase space contour plot of the proton distribution function for $T_\alpha/T_p = 1$ at $t = 336$, when the maximum of $\mathcal{E}$ is recovered in Figure 2(a). This contour plot displays the generation of a localized trapped particle region (delimited by the vertical white dashed lines) moving with mean velocity close to the phase speed of the IBk waves ($\sim 1.24 v_{\mathrm{th},p}$, black dashed line); this means that protons are trapped by the IBk waves. The surface plot of the phase space proton distribution in Figure 4(b) allows us to identify more clearly the region of trapped particles.

The presence of this trapped particle population affects the velocity distribution of protons. This is shown in Figure 4(c), where we plot the v_x–v_y level lines of the proton distribution function integrated over v_z and averaged over x in the spatial region of trapped particles (vertical white dashed lines in Figure 4(a)). Figure 4(d) shows the surface plot of the same distribution. Figures 4(c) and (d) give clear evidence of the generation of a well-defined field-aligned beam of protons moving with a mean velocity close to $V_A = 1$.

The effect of particle trapping by the IBk waves, which works for protons, cannot be efficient for alpha particles when $T_\alpha/T_p = 1$. In fact, in this case the thermal velocity of alpha particles is $v_{\mathrm{th},\alpha} = 0.25$, so that the phase speed of the IBk waves falls in the tail of the alpha particle velocity distribution

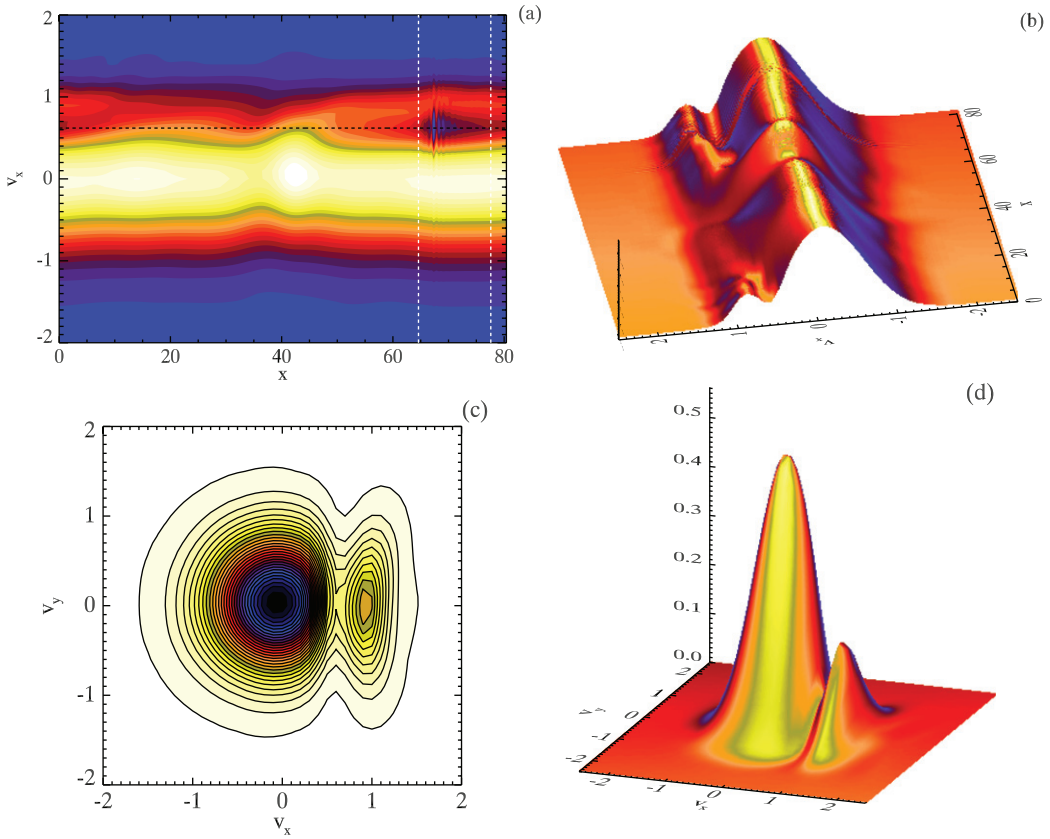

Figure 4. Protons: x–v_x level lines of the reduced distribution function (a) and surface plot (b), level lines of distribution function in the velocity plane v_x–v_y (c), and surface plot (d) at $t = 336$, for the case $T_e/T_p = 1$ and with $T_\alpha/T_p = 1$.

(A color version of this figure is available in the online journal.)

($v_\phi^{(\mathrm{IBk})} = 0.62 = 2.5 v_{\mathrm{th},\alpha}$). This means that, for T_α/T_p of the order of unity, trapping is less efficient for alpha particles than for protons. This is shown in Figure 5 (the same as Figure 4 for the alpha particles) where we point out that the alpha particle distribution function is modulated by the waves but no generation of beams is recovered.

In order to confirm the considerations above, we consider a simulation where we have increased the alpha particle to proton temperature ratio to the value $T_\alpha/T_p = 4$, in such a way that the two species have the same thermal speed $v_{\mathrm{th},p} = v_{\mathrm{th},\alpha} = 0.5$. In these conditions, the IBk waves can efficiently trap resonant alpha particles. The results of this new simulation are presented in Figure 6, where we show the v_x–v_y level curves (a) of the alpha particle velocity distribution integrated over v_z and averaged over x in the spatial region of trapped particles and the surface plot (b) of the same distribution. Here, we observe the generation of a field-aligned beam of alpha particles with mean velocity close to V_A. We point out that the behavior of protons is independent of the value of the alpha particle to proton temperature ratio.

The first set of simulations with $T_e/T_p = 1$ and $T_\alpha/T_p = 1, 4$ have shown that the branch of the IBk waves represents a preferential channel for carrying the energy from large to small scales in the longitudinal direction. Moreover, the Fourier analysis of the parallel electric energy from the simulations reveals that the phase speed of the IBk waves does not depend on T_α/T_p, at least for low values of the alpha particle to proton density ratio (we recall that $n_{0,\alpha}/n_{0,p} = 5\%$ in our simulations). Finally, the generation of a longitudinal beam of alpha particles is observed only when T_α/T_p is such that the condition $v_{\mathrm{th},p} \simeq v_{\mathrm{th},\alpha}$, for which trapping by IBk waves is efficient even for the alpha particles, is satisfied. The evidence that the field-aligned beam of alpha particles is observed in the simulations only for certain values of T_α/T_p could provide a possible explanation for the spacecraft observations discussed in Marsch (2010); in this paper the author points out that, at variance with the case of the solar-wind protons, for which a field-aligned beam is commonly observed, for the case of the alpha particles the generation of accelerated beams is a rare event.

When considering larger values of the electron to proton temperature ratio ($T_e/T_p = 5, 10$), the electrostatic activity recovered in the tail at short scales of the energy spectra displays slightly different features with respect to the case with $T_e/T_p = 1$. In Figure 7, we show the time evolution of $\mathcal{E}$ (as defined above) for two simulations with $T_e/T_p = 5, 10$ and with a fixed alpha particle to proton temperature ratio $T_\alpha/T_p = 1$ (the time evolution of $\mathcal{E}$ for $T_\alpha/T_p = 4$ is unchanged with respect to the case $T_\alpha/T_p = 1$). Here the exponential growing phase is visible, while the decreasing phase, observed for $T_e/T_p = 1$, is not recovered: indeed, after the growing phase, $\mathcal{E}$ saturates at a nearly constant level both for $T_e/T_p = 5$ and $T_e/T_p = 10$. The saturation value in the case $T_e/T_p = 10$ is larger than that at $T_e/T_p = 5$ by one order of magnitude. Except for the difference in the time evolution of $\mathcal{E}$, the simulations with $T_e/T_p = 5$ display a system dynamics similar to that discussed above for the case $T_e/T_p = 1$: in particular, the k–ω spectrum (not shown here) of the parallel electric energy in the case $T_e/T_p = 5$ again shows the presence of a single acoustic branch of IBk waves.

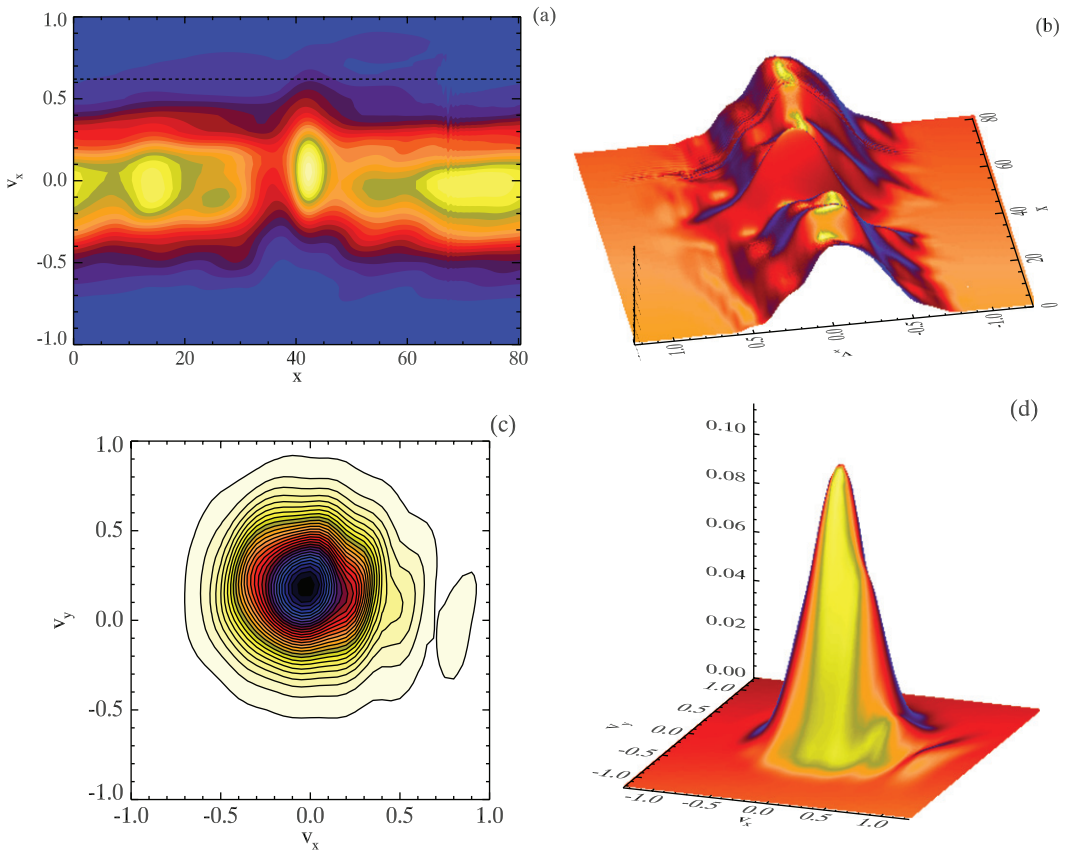

Figure 5. Alpha particles: x–v_x level lines of the reduced distribution function (a) and surface plot (b), level lines of distribution function in the velocity plane v_x–v_y (c), and surface plot (d) at $t = 336$, for the case $T_e/T_p = 1$ and with $T_\alpha/T_p = 1$.

(A color version of this figure is available in the online journal.)

On the other hand, this physical scenario is slightly changed for the case $T_e/T_p = 10$. In Figure 8, we show the numerical k–ω spectrum of the parallel electric energy for $T_e/T_p = 10$ and $T_\alpha/T_p = 1$ (the behavior is the same for the case $T_\alpha/T_p = 4$). For this value of electron to proton temperature ratio, unrealistic for the solar wind, we observe two branches of waves with different phase speeds: the lower branch of the IBk waves with $v_\phi^{(\mathrm{IBk})} \sim 1.24 v_{\mathrm{th},p}$ and the upper branch, consisting of ion-acoustic waves with $v_\phi^{(\mathrm{IA})} \sim 3.6 v_{\mathrm{th},p}$ (in agreement with the linear theory prediction). The generation of this branch of ion-acoustic waves is due to the fact that our initial perturbations do not satisfy the condition $B^2 = \mathrm{const.}$, so that quite soon in the simulations ponderomotive effects produce density fluctuations of the ion-acoustic type. For a large value of T_e/T_p these ion-acoustic fluctuations can survive against Landau damping (Krall & Trivelpiece 1986) and are visible in the k–ω, while for small T_e/T_p they are strongly dissipated.

4. SUMMARY AND DISCUSSION

In this paper, we have investigated the role of alpha particles in the development of the solar-wind turbulent cascade toward short wavelengths, in the direction parallel to the ambient magnetic field, by means of 1D-3V Eulerian hybrid Vlasov–Maxwell simulations.

We have shown that the presence of alpha particles does not influence the kinetic dynamics of protons (already discussed in previous works: Valentini et al. 2008, 2010; Valentini & Veltri 2009) occurring across the proton skin depth. During the system evolution the velocity distribution of protons exhibits significant deviations from local thermodynamic equilibrium. These deviations consist in the formation of a secondary proton beam moving in the direction of the background magnetic field $\mathbf{B}_0$ with mean velocity close to the local Alfvén speed, independent of the value of the electron to proton and alpha particle to proton temperature ratios.

The generation of this secondary beam is due to the fact that the IBk waves, the acoustic branch of waves which represent the main components of the electrostatic activity recovered at short scales, produce a localized trapped particle region in the proton distribution function, moving with mean velocity close to $v_\phi^{(\mathrm{IBk})}$. On the other hand, we have shown that the particle trapping by IBk waves is efficient for the alpha particles only when the thermal speed of alpha particles is close to that of protons ($v_{\mathrm{th},\alpha} \simeq v_{\mathrm{th},p}$), at least for a small number of alpha particles. When this condition is not respected, the alpha particle velocity distribution shows no distinct beams.

We point out that these numerical results can provide a possible explanation of a physical phenomenology discussed recently in Marsch (2010) and Bourouaine et al. (2011). In these papers, the authors show that in the solar-wind measurements from spacecraft the generation of a longitudinal beam of alpha particles appears to be a rare event with respect to a beam of protons. Through our numerical simulations we have demonstrated that a longitudinal beam of alpha particles is generated when $T_\alpha \simeq 4T_p$ (or, equivalently, $v_{\mathrm{th},\alpha} \simeq v_{\mathrm{th},p}$). According to the solar-wind data analysis by Kasper et al. (2008), the number of events in which $T_\alpha/T_p \simeq 4$ is somewhat

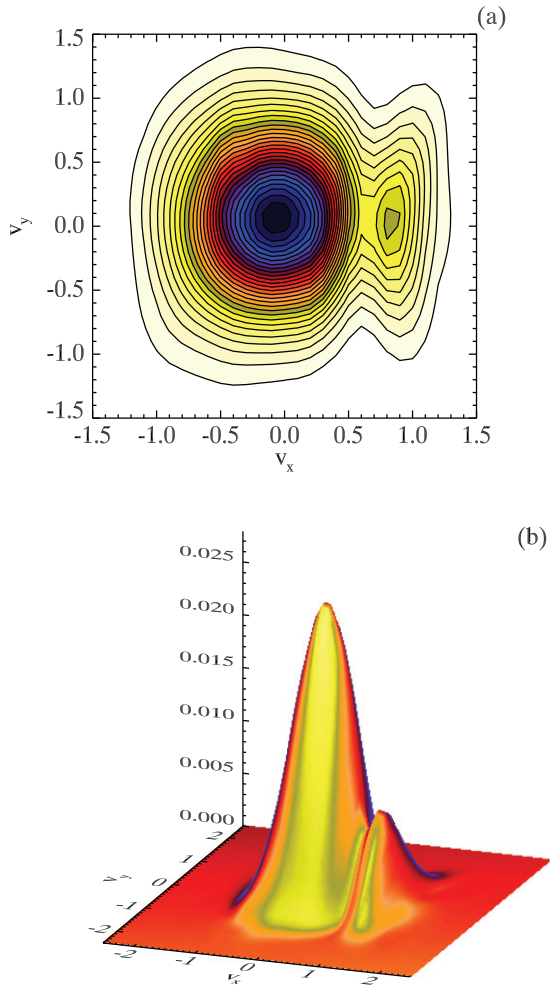

Figure 6. Alpha particles: level lines (a) and surface plot (b) of distribution function in the velocity plane v_x–v_y at $t = 328$, for the case $T_e/T_p = 1$ and with $T_\alpha/T_p = 4$.

(A color version of this figure is available in the online journal.)

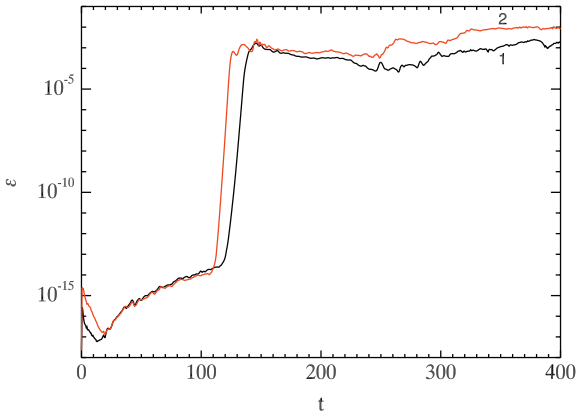

Figure 7. Time evolution of $\mathcal{E}$ in a semilogarithmic plot for the cases $T_e/T_p = 5$ (black line (1)) and $T_e/T_p = 10$ (red line (2)), with a fixed value of alpha particle to proton temperature ratio ($T_\alpha/T_p = 1$).

(A color version of this figure is available in the online journal.)

lower than the number of events with $T_\alpha/T_p \simeq 1$, meaning that the probability of observing the generation of a longitudinal beam of alpha particles is somewhat lower than the probability of detecting a proton beam.

Finally, concerning the particle heating problem, in our numerical simulations we found that in the early stage of system evolution, both proton and alpha particle distribution functions show perpendicular temperature anisotropy (perpendicular heating and parallel cooling). This process is more efficient for alpha particles than for protons, since in our simulations the energy is injected into the system along the left-hand branch that saturates asymptotically at the cyclotron frequency of the alpha particles.

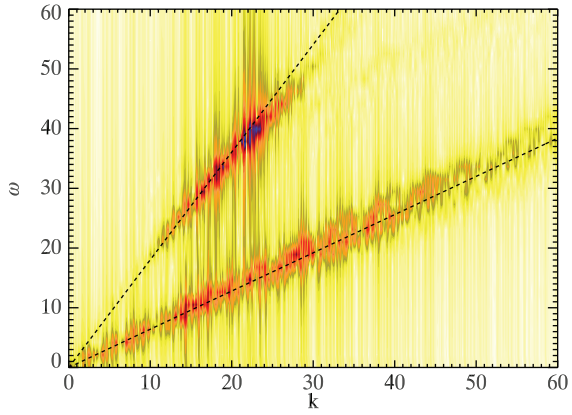

Figure 8. Numerical k–ω spectrum of parallel electric energy at $t = 400$, for the case $T_e/T_p = 10$ and with $T_\alpha/T_p = 1$. These two acoustic-like branches have different phase speeds: the lower branch of IBk waves with $v_\phi^{(\mathrm{IBk})} \sim 1.24 v_{\mathrm{th},p}$ and the upper branch of ion-acoustic waves with $v_\phi^{(\mathrm{IA})} \sim 3.6 v_{\mathrm{th},p}$.

(A color version of this figure is available in the online journal.)

The numerical simulations discussed in this paper were performed within the project SALPHVEN 2010, supported by the Italian SuperComputing Resource Allocation, ISCRA-CINECA, Bologna, Italy.

REFERENCES

Arunasalam, V. 1976, Phys. Rev. Lett., 37, 746
Bourouaine, S., Marsch, E., & Neubauer, F. M. 2011, ApJ, 728, L3
Busnardo-Neto, J., Dawson, J., Kamimura, T., & Lin, A. T. 1976, Phys. Rev. Lett., 36, 28
Dmitruk, P., Matthaeus, W. H., & Seenu, N. 2004, ApJ, 617, 667
Dusenbery, P. B., & Hollweg, J. V. 1981, J. Geophys. Res., 86, 153
Hansteen, V. H., Leer, E., & Holzer, T. E. 1997, ApJ, 482, 498
Hollweg, J. V., & Isenberg, P. A. 2002, J. Geophys. Res., 107, 1147
Isenberg, P. A. 1984, J. Geophys. Res., 89, 2133
Isenberg, P. A., & Hollweg, J. V. 1983, J. Geophys. Res., 88, 3923
Kasper, J. C., Lazarus, A. J., & Gary, S. P. 2008, Phys. Rev. Lett., 101, 261103
Krall, N. A., & Trivelpiece, A. W. 1986, Principles of Plasma Physics (San Francisco, CA: San Francisco Press)
Mangeney, A., Califano, F., Cavazzoni, C., & Trávníček, P. 2002, J. Comput. Phys., 179, 495
Marradi, L., Valentini, F., & Califano, F. 2010, Europhys. Lett., 92, 49002
Marsch, E. 2010, Space Sci. Rev., doi:10.1007/s11214-010-9734-z
Marsch, E., Goertz, C. K., & Richter, K. 1982, J. Geophys. Res., 87, 5030
Ofman, L. 2010, J. Geophys. Res., 115, A04108
Parashar, T. N., Shay, M. A., Cassak, P. A., & Matthaeus, W. H. 2009, Phys. Plasmas, 16, 032310
Peyret, R., & Taylor, T. D. 1986, Computational Methods for Fluid Flow (Berlin: Springer)
Schwenn, R., & Marsch, E. 1991, Physics of the Inner Heliosphere II. Particles, Waves and Turbulence, Vol. 2, 1st ed. (Berlin: Springer)
Valentini, F., Califano, F., Perrone, D., Pegoraro, F., & Veltri, P. 2011, Phys. Rev. Lett., 106, 165002
Valentini, F., Califano, F., & Veltri, P. 2010, Phys. Rev. Lett., 104, 205002
Valentini, F., Trávníček, P., Califano, F., Hellinger, P., & Mangeney, A. 2007, J. Comput. Phys., 225, 753
Valentini, F., & Veltri, P. 2009, Phys. Rev. Lett., 102, 225001
Valentini, F., Veltri, P., Califano, F., & Mangeney, A. 2008, Phys. Rev. Lett., 101, 025006
Xie, H., Ofman, L., & Viñas, A. 2004, J. Geophys. Res., 109, A08103